

**SMASIS2009-1368**

**SELF-CHARGING STRUCTURES USING PIEZOCERAMICS AND THIN-FILM BATTERIES**

**Steven R. Anton**

Department of Mechanical Engineering  
Virginia Polytechnic Institute and State University  
Blacksburg, VA 24061, USA

**Alper Erturk**

Department of Engineering Science and  
Mechanics  
Virginia Polytechnic Institute and State University  
Blacksburg, VA 24061, USA

**Na Kong, Dong S. Ha**

Department of Electrical and Computer  
Engineering  
Virginia Polytechnic Institute and State University  
Blacksburg, VA 24061, USA

**Daniel J. Inman**

Department of Mechanical Engineering  
Virginia Polytechnic Institute and State University  
Blacksburg, VA 24061, USA

**ABSTRACT**

This paper presents the investigation of a novel concept involving the combination of piezoelectrics and new thin-film battery technology to form multifunctional self-charging, load-bearing energy harvesting devices. The proposed *self-charging structures* contain both power generation and energy storage capabilities in a multilayered, composite platform consisting of active piezoceramic layers for scavenging energy, thin-film battery layers for storing scavenged energy, and a central metallic substrate layer. Several aspects of the design, modeling, fabrication, and evaluation of the self-charging structures are reviewed. A focus is placed on the evaluation of the load-bearing capabilities of the fabricated self-charging structures through both classical static failure testing as well as dynamic vibration failure testing.

**INTRODUCTION**

With recent growth in the development of low-power electronic devices such as portable consumer electronics and wireless sensor nodes, the topic of energy harvesting has received much attention in the research community. Several modes of energy harvesting exist including conversion of solar, thermal, vibration, and wind energy to electrical energy. Among these schemes, piezoelectric vibration-based harvesting has been most heavily researched [1, 2]. Previous studies have

investigated the modeling [3, 4], circuitry [5-7], and various applications [8-10] of vibration energy harvesting using piezoelectric devices. In this work, the authors investigate a novel multifunctional approach to piezoelectric energy harvesting in which additional functionality is achieved in a composite harvesting device.

Traditional piezoelectric energy harvesting systems consist of an active harvesting element, conditioning circuitry, and a storage medium, and the sole function of the entire system is to convert ambient mechanical energy into usable electrical energy. Furthermore, conventional systems are designed as add-on components to a host structure, often causing undesirable mass loading effects. In order to improve the functionality and reduce the adverse loading effects of traditional piezoelectric harvesting approaches, the authors propose a multifunctional energy harvesting design in which a single device can generate and store electrical energy and also carry structural loads. The proposed *self-charging structures*, shown in Figure 1, contain both power generation and energy storage capabilities in a multilayered, composite platform consisting of active piezoceramic layers for scavenging energy, thin-film battery layers for storing scavenged energy, and a central metallic substrate layer. The operational principle behind the device involves simultaneous generation of electrical energy when subjected to external dynamic loads causing deformations in the structure, as well as energy storage in the

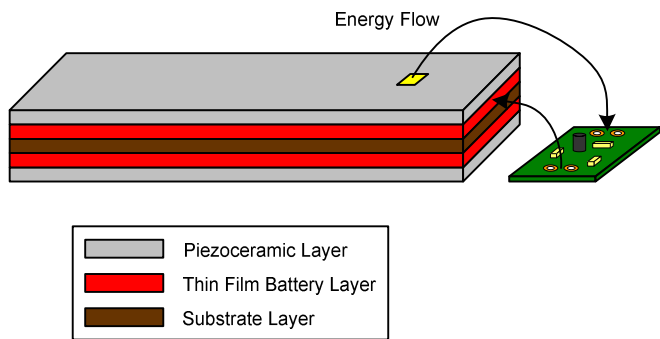


**Figure 1: Schematic of self-charging structure**

thin-film battery layers. Energy is transferred directly from the piezoceramic layers through appropriate conditioning circuitry to the thin-film battery layers, thus a single device is capable of both generating and storing electrical energy. Additionally, the self-charging structures are capable of carrying loads as structural members due to the flexibility of the piezoceramic and battery layers. The ability of the device to harvest energy, store energy, and support structural loads provides true multifunctionality.

The fruition of the self-charging structure concept is mainly due to the development of novel thin-film battery technology which allows for the creation of thin, flexible batteries. Conventional energy storage devices, such as capacitors and traditional rechargeable batteries, are not suitable for direct integration into the active element of an energy harvesting device as their mass and stiffness would hinder the ability to harvest energy. Additionally, they may fail under the loads applied to the harvester. Thin-film lithium-based batteries provide a viable solution with flexible devices that have thicknesses on the order of less than a millimeter, masses of around 0.5 grams, and capacities in the milliamp-hour range. Combined with an appropriate piezoelectric element and substrate layer, thin-film batteries can be used to create multifunctional self-charging structures.

The authors have recently introduced the concept of self-charging structures in which an electromechanical model is developed that can predict the performance of the device, and experiments are performed that confirm the ability of the device to both harvest and store energy [11, 12]. This paper gives an overview of the modeling and fabrication of the proposed self-charging structures, but focuses on the evaluation of the load-bearing capabilities of the device. The strength of the self-charging structures is investigated both statically through conventional three-point bending tests and dynamically by exciting the device at resonance under various excitation levels and monitoring for failure. Mathematical relations are given for the various strength calculations considered in this work. A mechanical model is given to determine the failure strength in three-point bending, and an electromechanically coupled model

is developed to predict the failure strength for the dynamic vibration testing. Details of the design and fabrication of the self-charging structures are outlined. Results from both the static and dynamic failure testing are given, and finally an efficient energy harvesting circuit topology is introduced.

## MATHEMATICAL BACKGROUND

A theoretical background for the *static mechanical* and *dynamic electromechanical* strength calculations of a thin self-charging beam is given in this section. For the three-point bending test, the static load required for brittle failure or ductile failure via a transition from elastic to plastic material behavior is considered in this work as the mechanical failure load that leads to the *mechanical failure strength*. For the dynamic vibration test, the base acceleration amplitude that corresponds to a prescribed electrical failure level (depending on the charge-discharge performance of the battery layers) is defined as the failure load (acceleration) that leads to the electrical failure strength of the self-charging structure. It is expected that in the dynamic testing, the devices will fail electrically before they fail mechanically, hence the dynamic failure strength is defined as an electrical failure strength. Expressions are derived in order to estimate the static and dynamic strength values in the following sections.

### Strength Calculations for Three-Point Bending Tests

Bending tests (or flexure tests) are usually employed to evaluate tensile strengths of brittle materials [13] (such as the piezoceramic layers in self-charging structures). The two basic types of bending tests are the three-point and four-point bending tests. The former type is used in this paper not only for the piezoceramic layers of the self-charging structure shown in Figure 2(a) but also for its other individual layers (Figure 2(b)), as well as for the two sections of the resulting self-charging assembly (Figure 2(c)). Details of the fabrication of the self-

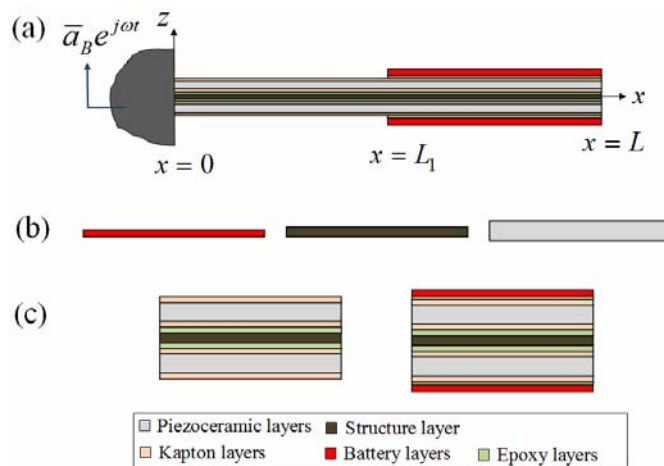


**Figure 2: (a) Self-charging structure showing all layers, (b) cross-sectional views of individual layers, and (c) cross-sectional views of the two sections of the assembly**

charging structure will be given in a later section.

A schematic of a classic three-point bending test setup is shown in Figure 3. The transverse load,  $P$ , is applied at the center ( $x = L/2$ ) of the uniform rectangular beam, therefore, the maximum bending moment occurs at this point ( $M_{\max} = PL/4$ ). Since not all the layers of the assembly (Figure 2(a)) are brittle, the term mechanical failure is again defined in this work as either a sudden drop in force for brittle failure or a transition from the elastic to plastic region in the load-deflection (or stress-strain) diagram for ductile failure. The maximum bending moment that corresponds to the failure load ( $P_f$ ) of the assembly is the failure bending moment ( $M_f$ ).

The maximum stress ( $T_k^{\max}$ ) of a layer in terms of the failure load of a multi-layer assembly can be given based on the Euler-Bernoulli beam theory as

$$T_k^{\max} = \frac{Y_k h_{kn}}{\bar{YI}} M_f = \frac{Y_k h_{kn} L}{4\bar{YI}} P_f \quad (1)$$

where  $h_{kn}$  is the distance from the neutral axis to the outer surface of the layer of interest (layer  $k$ ),  $Y_k$  is its elastic modulus, and  $\bar{YI}$  is the overall bending stiffness of the multi-layer beam. Equation (1) applies to the multi-layer cases of Figure 2(c) and it can be simplified to the following expression for a single-layer rectangular beam (Figure 2(b)):

$$T^f = \frac{hL}{8I} P_f = \frac{3L}{2bh^2} P_f \quad (2)$$

where  $h$  and  $b$ , respectively, are the total thickness and width of the single-layer beam. Note that, in order to obtain the bending stiffness ( $\bar{YI}$ ) of a multi-layer beam in Equation (1), a cross-section transformation (as described in Erturk and Inman [4]) can be used.

Equation (1) can be employed to estimate the maximum stresses of the individual layers for the failure load of the assembly, whereas Equation (2) gives the failure strengths of the individual layers under separate loading. It is worth mentioning that the maximum stress of a layer for the failure load of the assembly might be lower than its individual failure strength. For instance, for the failure load that results in fracture of a piezoceramic layer in a multi-layer assembly, the

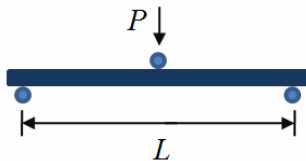


Figure 3: Schematic of a 3-point bending test setup

maximum stress in the metallic layer could be lower than its individual failure strength. Nevertheless, the overall structure is considered to be failed when it starts exhibiting brittle or ductile failure behavior.

### Strength Calculations for Dynamic Base Excitation Tests

Cantilevers used as piezoelectric energy harvesters are typically excited by the motion of their host structure (base excitation). Distributed-parameter analytical solutions for cantilevered unimorph [4], bimorph [14], and multi-morph [12] energy harvester beams have been presented in the recent literature. Convergence of the electromechanical Rayleigh-Ritz formulation [15] to the analytical solution given by Erturk and Inman [4] for sufficient number of kinematically admissible functions was reported in the literature [3]. Since the Rayleigh-Ritz formulation is an efficient way of handling structures with non-uniform geometric and material properties, the two-segment self-charging structure depicted in Figure 2(a) is modeled here using this technique. The following is a summary of the derivation (based on the Euler-Bernoulli beam theory) and details can be found in Hagood et al [15], Elvin and Elvin [3] or duToit et al [16] among others. The cantilevered beam structure is assumed to be sufficiently thin so that the shear strain and rotary inertia effects are negligible for the practical modes of interest (the fundamental mode is of particular interest in energy harvesting). The electrode pairs (of negligible thickness) covering the opposite faces of each piezoceramic layer are assumed to be perfectly conductive so that a single electric potential difference (voltage) can be defined across them.

The governing equations of a piezoelectric generator can be obtained from Hamilton's principle for electromechanical media as

$$\mathbf{M}\ddot{\mathbf{r}}(t) + \mathbf{C}\dot{\mathbf{r}}(t) + \mathbf{K}\mathbf{r}(t) - \mathbf{\Theta}v(t) = -\mathbf{M}^* a_B(t) \quad (3)$$

$$C_p \dot{v}(t) + \frac{v(t)}{R_l} + \mathbf{\Theta}^T \dot{\mathbf{r}}(t) = 0 \quad (4)$$

where  $\mathbf{M}$ ,  $\mathbf{C}$ , and  $\mathbf{K}$  are the mass, damping, and stiffness matrices,  $\mathbf{\Theta}$  is the electromechanical coupling vector,  $\mathbf{M}^*$  is the effective forcing vector,  $C_p$  is the equivalent capacitance,  $R_l$  is the external load resistance,  $\mathbf{r}(t)$  is the modal mechanical response,  $v(t)$  is the voltage response across the load resistance,  $a_B$  is the base acceleration of the harvester, and an over-dot represents differentiation with respect to time. Here, proportional damping is assumed so that standard modal analysis can be used with mathematical convenience (i.e., the damping matrix has the form  $\mathbf{C} = \alpha\mathbf{M} + \beta\mathbf{K}$  where  $\alpha$  and  $\beta$  are constants of proportionality). Expressions for the elements of the mass, stiffness, damping, effective forcing,

electromechanical coupling matrices, and vectors can be found in the literature [3, 15, 16].

The physical vibration response of the beam relative to its vibrating base is

$$w(x,t) = \sum_{i=1}^N \phi_i(x) r_i(t) = \mathbf{\Phi}^T(x) \mathbf{r}(t) \quad (5)$$

where  $\mathbf{\Phi}(x)$  is the vector of admissible functions and  $N$  is the total number of mechanical modes used in the expansion. A simple admissible function that satisfies the essential boundary conditions of a clamped-free beam is [3]

$$\phi_i(x) = 1 - \cos\left(\frac{(2i-1)\pi x}{2L}\right) \quad (6)$$

where  $i$  is the modal index. Note that one should use sufficient number of admissible functions for convergence of the natural frequencies of interest to the exact values.

If the base acceleration is assumed to be harmonic of the form  $a_B(t) = \bar{a}_B e^{j\omega t}$  (where  $\omega$  is the excitation frequency and  $j$  is the unit imaginary number), the steady-state voltage response and the vibration response can be obtained from

$$\begin{aligned} v(t) &= j\omega \left( \frac{1}{R_l} + j\omega C_p \right)^{-1} \mathbf{\Theta}^T \\ &\times \left( \mathbf{K} - \omega^2 \mathbf{M} - j\omega \mathbf{C} + j\omega \left( \frac{1}{R_l} + j\omega C_p \right)^{-1} \mathbf{\Theta} \mathbf{\Theta}^T \right)^{-1} \\ &\times \mathbf{M}^* \bar{a}_B e^{j\omega t} \end{aligned} \quad (7)$$

$$\begin{aligned} w(x,t) &= -\mathbf{\Phi}^T(x) \\ &\times \left( \mathbf{K} - \omega^2 \mathbf{M} - j\omega \mathbf{C} + j\omega \left( \frac{1}{R_l} + j\omega C_p \right)^{-1} \mathbf{\Theta} \mathbf{\Theta}^T \right)^{-1} \\ &\times \mathbf{M}^* \bar{a}_B e^{j\omega t} \end{aligned} \quad (8)$$

Here, the voltage output – to – base acceleration and the vibration response – to – base acceleration FRFs (frequency response functions) can be extracted as  $v(t)/\bar{a}_B e^{j\omega t}$  and  $w(x,t)/\bar{a}_B e^{j\omega t}$ , respectively.

The maximum dynamic stress of the  $k$ th layer of a thin self-charging structure under base excitation can be expressed as [12]

$$T_k^f(x_{cr}, t) = -Y_k h_{kn} \left. \frac{\partial^2 w(x,t)}{\partial x^2} \right|_{x=x_{cr}} + \lambda_k (\bar{e}_{31})_k \frac{v_k(t)}{h_{pk}} \quad (9)$$

where  $x_{cr}$  is the critical position on the beam where the curvature is maximum (e.g. it is the root for the fundamental mode of a uniform cantilever), the elastic modulus  $Y_k$  is the constant electric field modulus for a piezoceramic layer,  $(\bar{e}_{31})_k$ ,  $v_k(t)$ , and  $h_{pk}$  are the effective piezoelectric constant, voltage output, and thickness of the  $k$ th layer if it is a piezoceramic layer. Furthermore  $\lambda_k = 1$  if the  $k$ th layer is a piezoceramic layer, otherwise it is zero. From Equations (7) - (9), one can obtain the maximum dynamic stress FRF of the  $k$ th layer per base acceleration as  $T_k^f(x_{cr}, t)/\bar{a}_B e^{j\omega t}$ . Therefore, for a given value of base acceleration (such as the acceleration amplitude that results in a prescribed electrical failure condition), one can extract the maximum dynamic stress values of the individual layers. The maximum dynamic stress in the battery layer that corresponds to this prescribed electrical failure condition can be called the *electrical failure strength* of the battery under dynamic loading.

## FABRICATION OF SELF-CHARGING STRUCTURES

The components used to fabricate the self-charging structures used in this study, shown in Figure 4, consist of an 1100-O aluminum alloy substrate layer (colored blue on one face), QuickPack QP10N piezoelectric ceramic layers (Midé Technology Corp.), and Thinergy MEC101-7SES thin-film lithium battery layers (Infinite Power Solutions, Inc.). The QuickPack devices consist of a central monolithic piezoceramic (PZT-5A) layer bracketed by 0.0635 mm thick Kapton layers to protect the active element and provide some robustness. The Thinergy thin-film batteries are composed of a Lithium Cobalt Oxide (LiCoO<sub>2</sub>) cathode, metallic Lithium (Li) anode, and a solid state Lithium Phosphorous Oxy-Nitride (LiPON) electrolyte. The batteries have an operating voltage of 4.1 V and a capacity of 0.7 mAh. The important physical parameters of the various components used to construct the self-charging structures are given in Table 1.

Fabrication of the self-charging structures is performed by

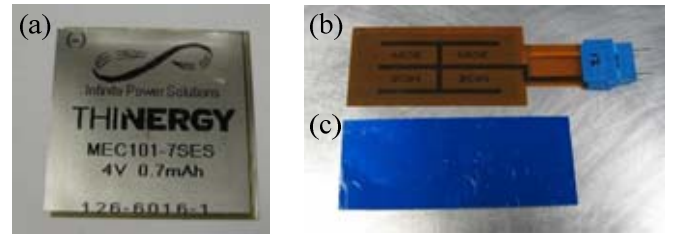


**Figure 4: (a) Thinergy MEC101-7SES battery, (b) QuickPack QP10N piezoceramic, (c) 1100-O aluminum alloy substrate**

**Table 1: Physical parameters of self-charging structure components**

Parameter	QP10N*			
	Aluminum Substrate	Active Element	QP10N Device	Thinergy Batteries
Thickness (mm)	0.127	0.254	0.381	0.178
Width (mm)	25.400	20.574	25.400	25.400
Length (mm)	63.500	45.974	50.800	25.400
Mass (g)	0.530		2.250	0.460

\* Dimensions for active piezo element only

separately bonding each layer using a vacuum bagging procedure (Figure 5(a)) to achieve thin, uniform bonding layers. 3M ScotchWeld™ DP460 2-part epoxy is chosen for the bonding layer due to its high shear strength (4000 psi when bonded to Aluminum) and high volume resistivity ( $2.4 \times 10^{14}$  ohm-cm). Bonding is achieved by applying a thin layer of epoxy between two structural layers, placing the device in vacuum, and allowing it to cure for 6 hours. After curing, any excess epoxy is removed from the edges of the device and the process is repeated until the self-charging structure is complete.

With all of the self-charging structure layers bonded, the final step in fabrication involves attaching electrical leads to both the piezoceramic layers and battery layers. The QuickPack devices contain an electrical connector (Figure 4(b)), however, it is removed to reduce the length and mass of the piezoceramic layer. With the connector removed, a small area of the flat electrodes is exposed by removing the Kapton coating with a razor blade. 22-gauge insulated and stranded wire is then soldered to the exposed electrodes to create an electrical connection. The entire faces of the Thinergy batteries serve as electrodes, and there is a slight overlap on one of the sides of the battery such that both positive and negative electrodes are accessible from one side of the battery. Electrical leads are attached to the batteries by directly soldering the same 22-gauge wire to the electrode surfaces. A very small amount

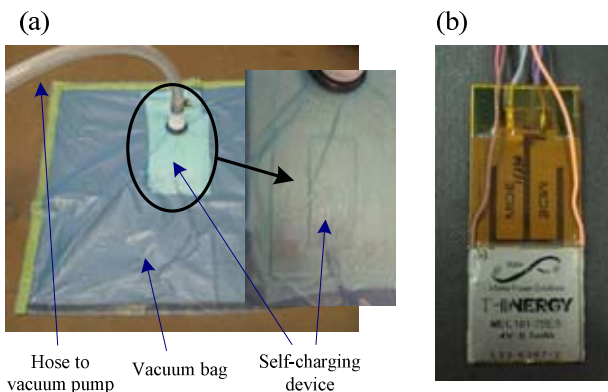


**Figure 5: (a) Vacuum bagging setup, (b) complete self-charging structure**

of solder is used as to not short the device when attaching the lead to the overlapping electrode, therefore, an additional epoxy coating is placed over the electrode connections to provide mechanical strength as well as electrical insulation. Loctite 3381 UV curable epoxy is used to coat the connection points and is cured in about 3 minutes using UV LED light. A photograph of a complete self charging structure with electrical leads can be seen in Figure 5(b).

## FAILURE ANALYSIS

### Static Failure Testing

In order to characterize the bending strength of the complete self-charging structure as well as the individual component layers, three-point bending tests are performed using an Instron 4204 universal test frame equipped with a 1000 N load cell and a small three-point bend fixture with adjustable supports, shown in Figure 6(a). Each specimen rests on the two lower support pins, which are spaced 20 mm apart, and the central pin is lowered using the machine at a rate of 0.3 mm/min until a prescribed displacement is reached. In each case, the specimens fail before the maximum displacement is achieved.

Three individual samples are tested for the aluminum substrate, QP10N piezoceramic, and Thinergy battery layers. Aluminum specimens are cut to 25.4 mm x 25.4 mm, and the QuickPack samples are cut in half (resulting in about 25.4 mm x 25.4 mm) to fit in the test fixture. A single self-charging structure is tested and cut in half such that each section can be

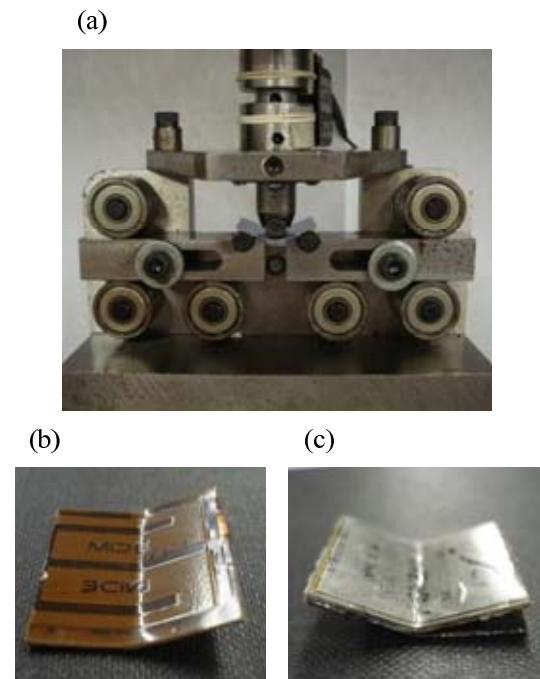


**Figure 6: (a) Three-point bending fixture, self-charging structure sections after failure testing for (b) root section, (c) tip section**

tested separately. Photographs of the two self-charging sections after failure testing are shown in Figure 6(b) and Figure 6(c). The load and crosshead displacement are recorded throughout each test, and typical load-deflection curves for the individual layers as well as the complete structure are shown in Figure 7. The failure load is defined in this work as a transition from the elastic to plastic region in the load-deflection diagram for the specimens exhibiting ductile behavior (aluminum substrate, Thinergy battery, self-charging structure tip section), and as the point at which the first drop in force is observed for specimens exhibiting brittle failure (QuickPack piezoceramic, self-charging structure sections). From the results presented in Figure 7(a), it is clear that the individual QuickPack piezoceramic layers exhibit brittle failure and the individual aluminum substrate and Thinergy battery layers exhibit ductile failure. In the case of the aluminum sample, the failure load is taken where a slight, prolonged drop in the force is observed, as noted in the figure. From Figure 7(b), it can be seen that the root section of the self-charging structure experiences brittle failure, where the tip section exhibits simultaneous ductile and

**Table 2: Failure loads for three-point bending tests**

Parameter	Aluminum Substrate	QP10N Piezoceramic	Thinergy Batteries
Failure Load (N)	3.21	7.25	6.58
	3.36	8.80	5.47
	3.66	8.50	5.89
Minimum (N)	3.21	7.25	5.47
<b>Complete Self-Charging Structure</b>			
	<u>Root Section</u>		<u>Tip Section</u>
Failure Load (N)	39.9		165.3

brittle failure signatures. This phenomenon is likely due to failure occurring in the piezoceramic and battery layers for nearly the same force. The failure load results for all of the specimens tested are presented in Table 2.

With the failure loads obtained, the previously described *mechanical failure strength* (stress in each layer at failure) can be obtained by substituting the appropriate values from Table 1 and Table 2 into Equations (1) and (2). The minimum failure load value is used in the calculations for the individual layers to give a conservative estimate. For the complete self-charging structure, the overall bending stiffness ( $\bar{YI}$ ) of the root section (containing only the aluminum substrate and QuickPack piezoceramic layers) is calculated as  $\bar{YI} = 0.0652 \text{ N/m}^2$ , and of the tip section (containing the aluminum substrate, QuickPack piezoceramic layers, and battery layers) is calculated as  $\bar{YI} = 0.1960 \text{ N/m}^2$ . It should be noted that the calculation of failure stress in the QP10N piezoceramic layers considers the dimensions of only the active element, ignoring the Kapton as the ceramic experiences brittle failure. The calculated failure strength values for each of the specimens are

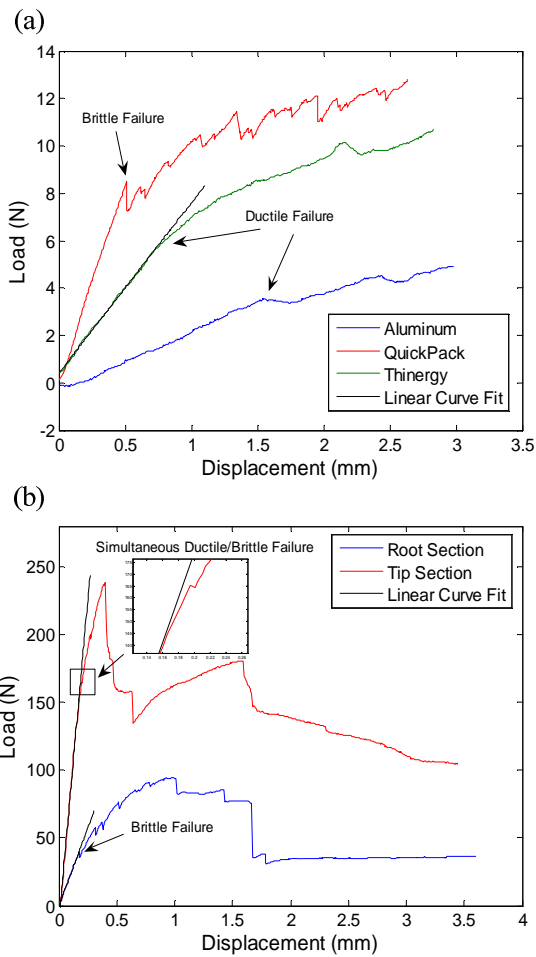


**Figure 7: Load-deflection curves for (a) individual layers and (b) complete self-charging structure sections**

**Table 3: Maximum stress at failure for three-point bending tests**

Parameter	Aluminum Substrate	QP10N Piezoceramic	Thinergy Batteries
<b>Individual Layers</b>			
Failure Stress (MPa)	229.27	159.82	199.33
<b>Self-Charging Structure - Root Section</b>			
Failure Stress (Mpa)	14.62	99.57	N/A
<b>Self-Charging Structure - Tip Section</b>			
Failure Stress (Mpa)	20.15	137.23	155.44

given in Table 3.

From the results it can be seen that failure in the root section of the self-charging structure is due to failure of the piezoceramic layers. At the point of failure, the maximum stress in the aluminum layer is much less than the failure stress observed in a single aluminum layer. The failure stress in the QuickPack is about half of the failure stress obtained for a single layer, however, it is on the same order of magnitude. Although there is a significant difference between the failure stress of the single layer and composite device, it is typical in brittle failure to observe a wide range of failure loads (thus stresses) for a single material. The results for the tip section of the self-charging structure show failure in both the piezoceramic and battery layers with stresses similar to the failure stress of the individual layers in both cases. This result is confirmed by the simultaneous brittle and ductile failure observed in Figure 7(b). Overall, it can be concluded that the piezoceramic and battery layers are the critical layers in three-point bending failure.

### Dynamic Failure Testing

To gain an understanding of the dynamic loading that can be withstood by the self-charging structures without failure, a series of dynamic tests are conducted with the device mounted in a cantilever configuration on a small TMC Solution Dynamic TJ-2 electrodynamic shaker, as shown in Figure 8(a). The dynamic failure testing is conducted by subjecting the cantilevered harvester to resonant base excitations of increasing amplitude until electrical failure is observed. Electrical failure is defined as a 10% decrease in either the charge or discharge behavior of the device as compared to baseline charge/discharge curves. Prior to the dynamic testing, a self-charging structure is clamped with an overhang length of 43.7 mm and mounted on the shaker. The device is not disturbed for the duration of testing.

In order to determine the resonant frequency and optimal load resistance of the clamped device, experiments are conducted to obtain the electromechanical FRFs of the self-charging structure for a set of resistive electrical loads (ranging from 100  $\Omega$  to 1 M $\Omega$ ). SigLab data acquisition hardware is

used for all FRF measurements. The input acceleration is measured using a PCB U352C67 accelerometer, the tip displacement is measured using a Polytec OFV303 laser Doppler vibrometer, and the voltage output of the device is measured directly with the data acquisition system. The overall test setup is shown in Figure 8(b). For the series connection of the piezoceramic layers (to obtain larger voltage output), the voltage output – to – base acceleration FRFs and the tip velocity response – to – base acceleration FRFs of the symmetric multi-layer generator are shown in Figure 9(a) and Figure 9(b), respectively (where the base acceleration is given in terms of the gravitational acceleration,  $g = 9.81 \text{ m/s}^2$ ).

To verify the electromechanical model used for the calculation of dynamic strength, the voltage output and the vibration response FRFs are predicted using Equation (7) and Equation (8), respectively, and plotted over the experimental results in Figure 9. 20 modes are used in the Rayleigh-Ritz formulation ( $N = 20$ ) to ensure the convergence of the fundamental natural frequency using the admissible functions given by Equation (6). As the load resistance is increased from 100  $\Omega$  to 1 M $\Omega$ , the experimental value of the fundamental resonance frequency moves from 204 Hz (close to short-circuit conditions) to 211.1 Hz (close to open-circuit conditions). These two frequencies are called the short-circuit and the open-circuit resonance frequencies [4, 14] and they are predicted by the electromechanical model as 204.1 Hz and 211 Hz, respectively. The amplitude-wise model predictions are also in agreement with the experimental measurements. It is worth mentioning that the maximum voltage output is obtained for the largest load resistance for excitation at the open-circuit resonance frequency as 34 V/g (peak amplitude). The optimal electrical loads for excitations at 204 Hz and 211.1 Hz are identified as 9.8 k $\Omega$  and 91 k $\Omega$  (among the resistors used), respectively, which yield similar peak power outputs of 2.8 mW/g<sup>2</sup> and 3.1 mW/g<sup>2</sup>, respectively. These voltage and power output values given in terms of base acceleration are, however, frequency response-based linear estimates obtained from low-amplitude chirp excitation and they are not necessarily accurate for large-amplitude excitations with nonlinear response characteristics.

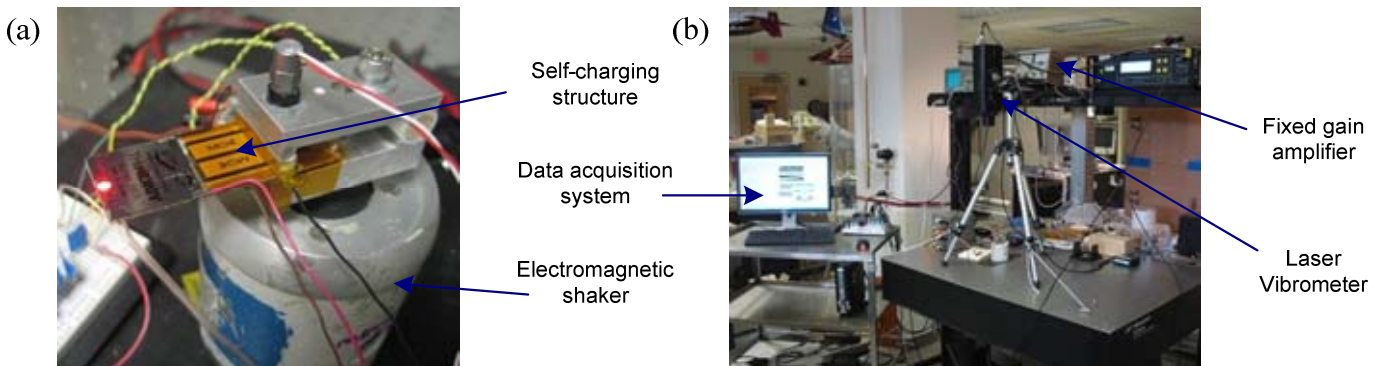
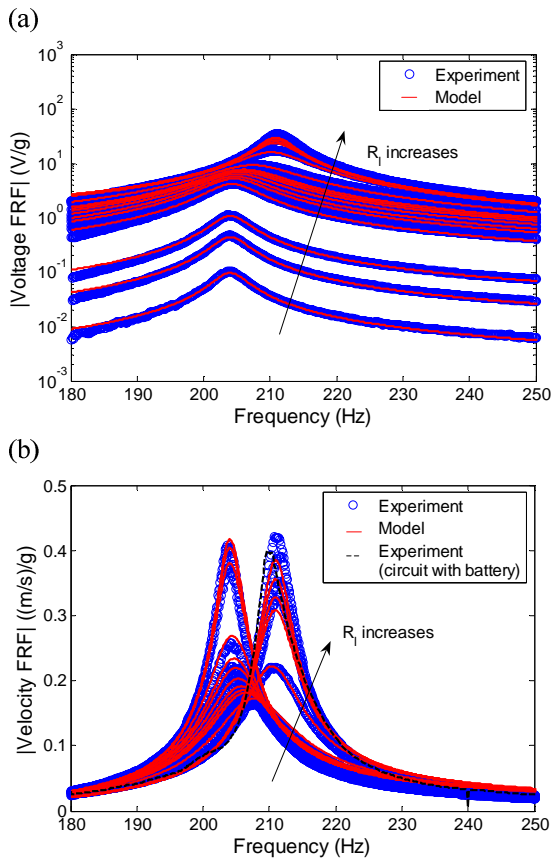


Figure 8: (a) Self-charging structure mounted to shaker and (b) overall experimental setup for dynamic testing

After the preliminary analysis for the resistive load case, the piezoceramic and thin-film battery layers are connected to the input and output of the regulator circuit, respectively. The electrical boundary conditions of the piezoceramic layers then become more sophisticated. The tip velocity FRF is measured for this case as well and plotted in Figure 9(b). It appears from the figure that the case with the largest resistive load (1 MΩ, close to open-circuit conditions) represents the vibration response of the self-charging structure around the fundamental resonance frequency (210 Hz) successfully. Therefore, the dynamic (mechanical) behavior of the self-charging structure close to open-circuit conditions (with 1 MΩ) is taken as the basis for the strength calculations. Indeed considering the open-circuit condition case where the shunt damping effect is the least (just like in the short-circuit case) is a conservative way of estimating the dynamic bending stress in the structure layers.

Equation (9) is used in order to obtain the maximum dynamic stress FRFs of the aluminum, piezoceramic and battery layers per base acceleration input. The average epoxy thickness between the piezoceramic and aluminum layer is measured as 0.0173 mm whereas the average epoxy layer thickness between the outer Kapton and the battery layers is negligible. The



**Figure 9:** The (a) voltage-to-base acceleration FRFs and (b) tip velocity-to-base acceleration FRFs of the self-charging structure for a set of resistors

distances ( $h_{kn}$ ) from the neutral axis of the symmetric structure to the outer surfaces of the aluminum, piezoceramic and battery layers are then estimated as 0.0635 mm, 0.398 mm and 0.614 mm, respectively. The elastic moduli ( $Y_k$ ) of these structures are taken as 70 GPa, 69 GPa and 55 GPa. Since the aluminum and piezoceramic layers are clamped at the root, the maximum stresses for these layers are expected to be at the root (i.e.  $x_{cr} = 0$  in Equation (9)). However, since the 25.4-mm-long battery layers are located close to the free end, the maximum stress in the battery layers is expected to be at  $x_{cr} = 18.3$  mm. With this information, the maximum stress – to – base acceleration FRFs are calculated and plotted in Figure 10. The maximum bending stress per base acceleration of the aluminum, piezoceramic and battery layers are 5.7 MPa/g, 20.5 MPa/g and 3.1 MPa/g.

With the resonance frequency of the self-charging structure connected to the circuit obtained (210 Hz), the dynamic failure testing can be performed. The metric for determining electrical failure (recall it is expected that the device will fail electrically before it fails mechanically) is a 10% change in the charge or discharge behavior compared to a baseline. This method is similar to that proposed in [17-19] where the performance of similar thin-film batteries under static loading and embedded in carbon fiber reinforced composite structures is investigated. Charging is performed using a constant voltage charging method by supplying 4.1 V to the battery using a power supply until only about 35 μA of current is sourced by the battery. Discharging is performed by applying a resistive load of 2749 Ω across the battery in order to draw roughly 2C of current (2 times the rated 0.7 mAh capacity, i.e. 1.4 mA) until a voltage of 3.0 V is reached. Both the battery current and voltage are recorded throughout each test. By integrating the current over time during charging and discharging, the amount of energy flowing through the battery can be quantified in terms of a capacity in milliamp-hours (mAh). Changes in this calculated capacity will be used to identify electrical failure of the structure.

Before the self-charging structure is ever excited

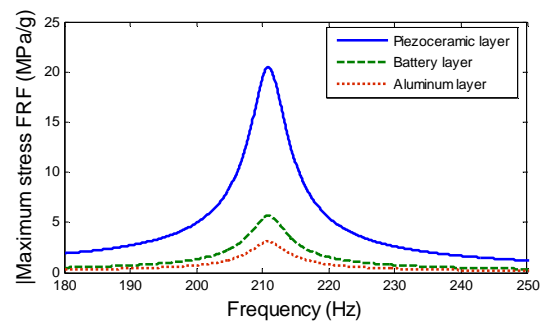


**Figure 10:** Estimates of the maximum dynamic bending stress in the piezoceramic, battery, and aluminum layers per base acceleration input

mechanically, a baseline charge/discharge profile is obtained. All future measurements are compared to this baseline. The dynamic failure testing is performed using the following steps. First, the device is excited at resonance at an initial acceleration input level of  $\pm 0.2 g$  for 1 hour. During the test, the piezoceramic layers are connected in series to the harvesting circuit and used to charge a single thin-film battery (which is initially fully discharged to 3.0 V). The battery voltage and current are monitored and recorded. After 1 hour, the excitation is ceased and a discharge test is performed on the battery. The self-charging structure is then allowed to sit for 24 hours before testing is resumed. The following day, the thin-film battery is charged using the power supply and then discharged. This data is compared to the baseline charge/discharge curves, and significant changes indicate device failure (caused by the excitation the previous day). Finally, the acceleration amplitude is increased and the process is repeated. Typical curves for both the power supply and piezoceramic charge/discharge tests are shown in Figure 11. Complete results from the dynamic failure testing for the power supply charge/discharge are given in Figure 12(a) for base acceleration values from 0.2 g to 7.0 g. Additionally, the complete charge/discharge results with the piezoceramic layers charging the battery are given in Figure 12(b).

From the dynamic failure testing results presented in Figure 12(a), it can be seen that as the excitation amplitude is increased from 0.2 g to 7.0 g, there is no significant change in the power supply charge or discharge behavior. In each case, the charge amplitude is slightly higher than the discharge amplitude, likely due to leakage in the battery. The power supply charge at 5.5 g is abnormally high, thus the battery

initially looks damaged, but continuation of testing at higher excitation levels shows that the battery still functions properly. This phenomenon may be due to experimental errors. Although it was expected that electrical failure would occur before mechanical failure, no electrical failure was observed. Testing is stopped at an excitation level of 7.0 g in order to protect the device from any mechanical failure. According to the maximum stress predictions given in Figure 10, 7.0 g of excitation corresponds to roughly 145 MPa in the piezoceramic layer, 22 MPa in the battery layer, and 40 MPa in the aluminum substrate. Recall that the piezoceramic layers were found to fail statically between 100 - 140 MPa for the complete self-charging structure assembly. Although the static and dynamic failure strengths are not expected to be the same, the stress in the piezoceramic layers at 7.0 g may be close to the dynamic mechanical failure strength.

The piezoceramic charge/discharge results presented in Figure 12(b) show that the piezoceramic layers are able to partially charge the thin-film battery. As the excitation amplitude is increased, the total charge capacity monotonically increases. This is expected as more vibration energy is available for harvesting at higher excitation levels. Accordingly, the discharge capacity also increases with the excitation amplitude. There is, however, a difference in the charge and discharge capacities for each test. This variability is likely due to leakage in the battery as the current input from the piezoceramic layers is quite low. Overall, these results are in

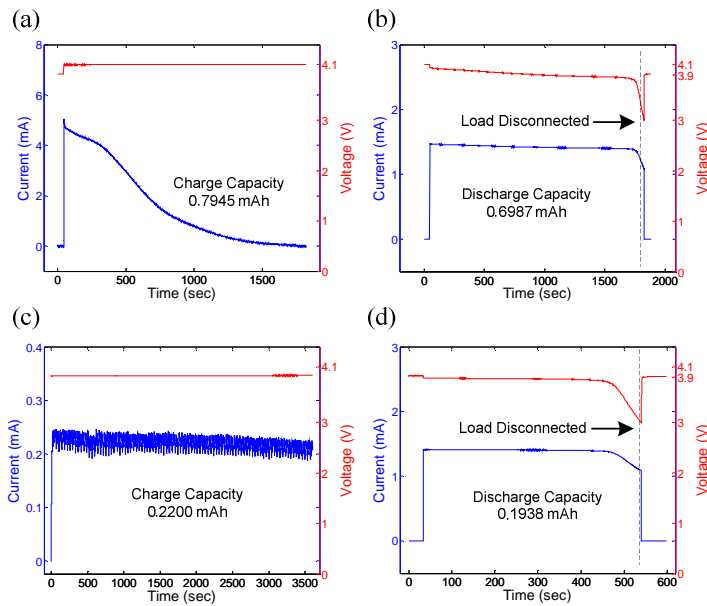


**Figure 11: Typical charge/discharge curves for power supply (a) charge and (b) discharge at 0.6 g, and piezoceramic (c) charge and (d) discharge at 5.5 g**

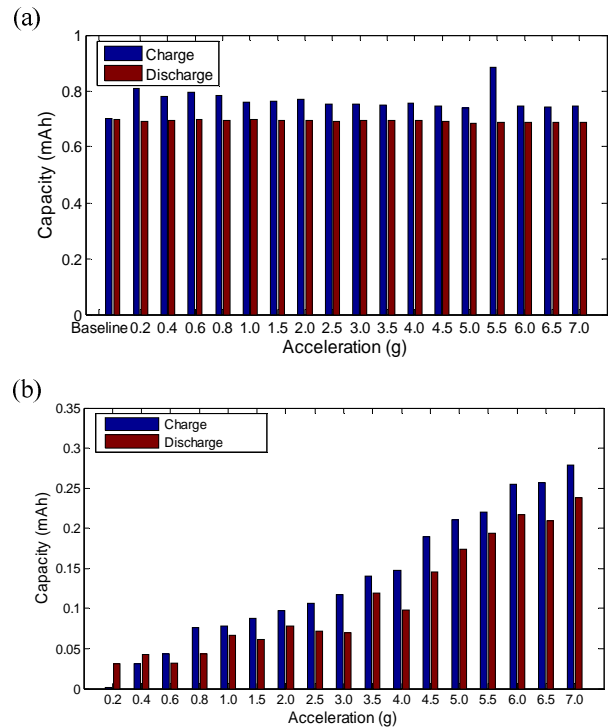


**Figure 12: Charge/discharge capacities measured for (a) power supply and (b) piezoceramic charging**

agreement with the power supply results in that no electrical failure is observed for any of the excitation levels tested.

Previous studies by Pereira et al. [17, 18] have investigated the strength of NanoEnergy thin-film batteries (Front Edge Technology, Inc.) under static loading. In three-point bending, it is found that both mechanical (delamination) and electrical (drop in charge/discharge performance) failure occur for flex ratios (defined as the deflection divided by the span length) greater than 1.3%. When subjected to uniaxial pressure, the batteries are found to fail at pressures greater than 2.0 MPa. It was expected that similar failure would be observed for the self-charging structures using Thinergy batteries in the dynamic loading case. Overall, the self-charging structures have proven to be robust and it appears that dynamic electrical failure from large amplitude base excitations is unlikely.

### IMPEDANCE MATCHING ENERGY HARVESTING CIRCUIT

To convert the raw AC power from the piezoelectric harvester to a stable DC power required to power a load or, in this case, store the scavenged energy into the thin-film battery, an efficient power conditioning circuit is indispensable for energy harvesting. A rectifier followed by a linear voltage regulator was previously proposed by the authors for use with self-charging structures and is used in the dynamic failure testing in this study [11]. Considering the importance of impedance matching for maximum power transfer, a new approach is implemented to increase the efficiency of power extraction. A nonlinear switching circuit whose parameters can be tuned to allow for impedance matching is proposed. The circuit schematic is shown in Figure 13. A diode-bridge is used as the first stage to rectify the AC output of the piezoelectric element to DC. The second stage is a buck-boost converter designed to run in discontinuous conduction mode. The switching frequency of the switch is much higher than the base excitation frequency. During each switching period, the input voltage to the buck-boost converter can be treated as a stable DC voltage. The voltage and current waveforms during a

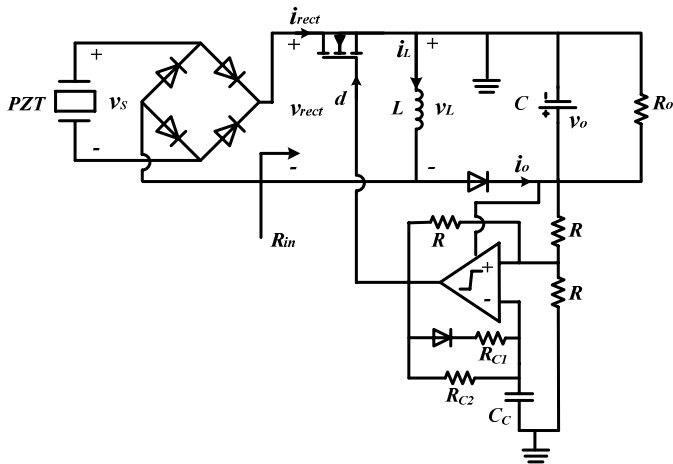


Figure 13: Schematic of the energy harvesting circuit

switching period are shown in Figure 14.

There are three intervals in a switching cycle. In the first interval,  $D_1 T_s$ , the switch turns on. The piezoceramic elements charge the inductor and the inductor current increases with a slope of  $v_{rect}/L$ . In the second interval,  $D_2 T_s$ , the switch turns off. The inductor is discharged through the load and the inductor current decreases with a slope of  $v_o/L$  until it reaches zero. During the rest of the switching cycle, the switch remains off and the inductor current remains at zero. The advantage of this circuit is that the input impedance of the DC-DC converter is inherently a resistance [20] with the value given by

$$R_{in} = \frac{v_{rect}}{\frac{1}{T_s} \int_0^{D_1 T_s} i_L dt} = \frac{v_{rect}}{\frac{1}{T_s} \int_0^{D_1 T_s} \frac{v_{rect}}{L} t dt} = \frac{2L}{D_1^2 T_s} \quad (10)$$

where  $v_{rect}$  is the rectified voltage,  $L$  is the inductor value,  $i_L$  is the current through the inductor,  $T_s$  is the switching period, and  $D_1$  is the duty cycle. By adjusting the duty cycle of the gate signal for the switch, the optimal resistive load can be emulated by the buck-boost converter as given by

$$D_{1,opt} = \sqrt{\frac{2L}{R_{in,opt} T_s}} \quad (11)$$

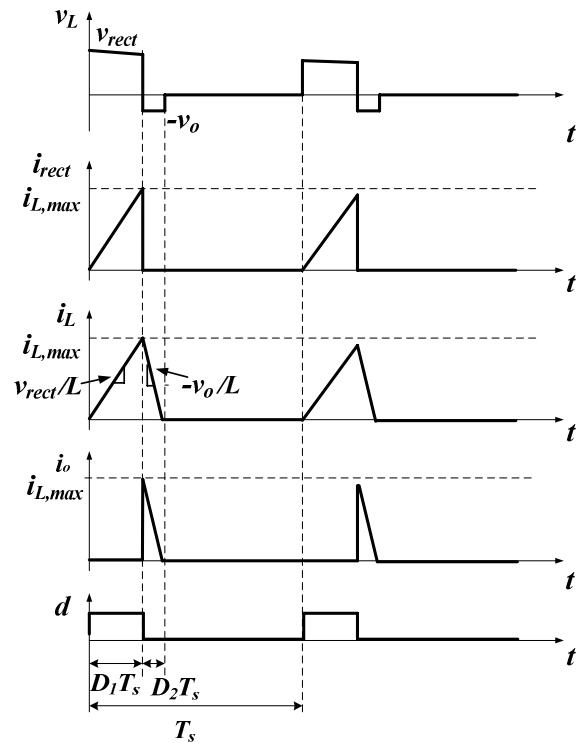


Figure 14: Waveforms during one switching period

The output power is not a function of the load. More details about the resistive impedance matching circuit can be found in [21].

Experiments are performed to determine the efficiency of the linear regulator circuit used for the dynamic testing and the proposed switching-mode impedance matching circuit. In order to calculate the efficiency of the circuits, a reference value must first be obtained experimentally. Additionally, the input mechanical energy must be held constant for each test. An input acceleration amplitude of 2.0 *g* is selected for testing. The baseline measurement will be taken with the self-charging structure (piezoceramic layers in series) connected to an optimal load resistance. This case represents the maximum available energy that can be extracted from the piezoceramic layers. When applying base excitations with an amplitude of 2 *g* to the piezoelectric harvester at the open-circuit resonance frequency of 211.1 Hz, 1.6 mW of average power (recall the unconditioned piezoelectric output is AC) is measured across the optimal resistive load of 85 k $\Omega$ . An average power of 1.6 mW, therefore, becomes the baseline power value for evaluating the performance of the two harvesting circuits.

With the baseline measurement obtained, the efficiency of the two harvesting circuits can be tested. In each case, the energy transferred from the piezoceramic layers to a CapXX GW209F 0.12 Farad, 4.5 V supercapacitor will be used as a measure of power. The capacitor is initially pre-charged to a voltage of 3.0V and the voltage increase over a set amount of time results in an average power that can be compared to the baseline power to determine the efficiency. It should be noted that the self-discharge rate of the supercapacitor is measured and taken into consideration for the power calculations. The linear regulator circuit is tested first. FRF measurements have previously been taken with the self-charging structure connected to this circuit and a resonance of 210 Hz was found. When exciting at a base acceleration amplitude of 2.0 *g* at 210 Hz, the average power delivered to the supercapacitor is measured to be 493  $\mu$ W. This results in an efficiency of 30% when compared against the available power of 1.6 mW for the baseline case.

The new switching circuit is tested next. Due to the impedance matching of the switching circuit, the resonance frequency with the self-charging structure connected to the circuit is the same as the optimal resistance case (211.1 Hz). Exciting the structure at 211.1 Hz and a base acceleration amplitude of 2.0 *g* yields a power of 862  $\mu$ W delivered to the supercapacitor, which results in a greatly increased overall efficiency of 53.8% as compared to the linear circuit. It should be noted that if the available power is much lower, the power loss in the relatively complex switching-mode circuit may overwhelm the efficiency gain from the impedance matching compared to the linear voltage regulator. The appropriate circuit should be selected based on the operation conditions of the harvester.

## SUMMARY AND CONCLUSIONS

The strength of the proposed self-charging structures has been investigated under both static and dynamic loading. Expressions are first derived to predict the maximum stress in each structural layer for a given failure load in three-point bending as well as the maximum stress in each layer under for a given base excitation acceleration amplitude under dynamic loading. Experiments are then carried out to test the strength of the self-charging structures. Three-point bending tests are first performed on several individual layers as well as each section of a complete device. Results from the static testing show that the piezoceramic and battery layers are the critical layers in bending failure, with both layers failing at nearly the same load in the tip section of the self-charging structure. Dynamic failure testing is next performed where the device is subjected to base excitations of increasing amplitude at resonance. The dynamic testing results both confirm the ability of the piezoceramic layers to charge the thin-film battery layers and show that electrical failure of the battery is not experienced up to 7.0 *g* of excitation, which approaches the critical amplitude for mechanical failure in the piezoceramic layers. Lastly, an efficient impedance matching energy harvesting circuit that operates on a switching-mode power conversion principle is introduced. The efficiencies of the switching circuit as well as the linear regulator circuit used during the dynamic tests are measured experimentally and it is found that a significant increase can be obtained with the impedance matching circuit for sufficiently high input powers. Overall, the failure strength values found in this research are promising. The self-charging structures have proven to be robust under dynamic loading at resonance. Electrical failure is not experienced and the mechanical failure strength values are reasonable.

## ACKNOWLEDGMENTS

The authors would like to acknowledge the help of Mac McCord from the Department of Engineering Science and Mechanics at Virginia Tech during three-point bend testing. The authors also gratefully acknowledge the support of the Air Force Office of Scientific Research MURI under Grant No. F9550-06-1-0326 "Energy Harvesting and Storage Systems for Future Air Vehicles" monitored by Dr. B. L. Lee.

## REFERENCES

- [1] Anton, S. R. and Sodano, H. A., (2007) "A review of power harvesting using piezoelectric materials (2003-2006)," *Smart Materials and Structures*, **16**(3), pp. R1-R21.
- [2] Cook-Chennault, K. A., Thambi, N., and Sastry, A. M., (2008) "Powering MEMS portable devices-a review of non-regenerative and regenerative power supply systems with special emphasis on piezoelectric energy harvesting systems," *Smart Materials and Structures*, **17**(4), pp. 043001 (33 pp.).

- [3] Elvin, N. G. and Elvin, A. A., (2009) "A general equivalent circuit model for piezoelectric generators," *Journal of Intelligent Material Systems and Structures*, **20**(1), pp. 3-9.
- [4] Erturk, A. and Inman, D. J., (2008) "A distributed parameter electromechanical model for cantilevered piezoelectric energy harvesters," *Journal of Vibration and Acoustics*, **130**(4), pp. 041002 (15 pp.).
- [5] Lallart, M., Garbuio, L., Petit, L., Richard, C., and Guyomar, D., (2008) "Double synchronized switch harvesting (DSSH): A new energy harvesting scheme for efficient energy extraction," *IEEE Transactions on Ultrasonics, Ferroelectrics, and Frequency Control*, **55**(10), pp. 2119-2130.
- [6] Lefeuvre, E., Audigier, D., Richard, C., and Guyomar, D., (2007) "Buck-boost converter for sensorless power optimization of piezoelectric energy harvester," *IEEE Transactions on Power Electronics*, **22**(5), pp. 2018-2025.
- [7] Yiming, L., Geng, T., Yong, W., Junhong, L., Qiming, Z., and Hofmann, H. F., (2009) "Active Piezoelectric Energy Harvesting: General Principle and Experimental Demonstration," *Journal of Intelligent Material Systems and Structures*, **20**(5), pp. 575-585.
- [8] Anton, S. R. and Inman, D. J., (2008) "Vibration energy harvesting for unmanned aerial vehicles," in *SPIE's 15th Annual International Symposium on Smart Structures and Materials & Nondestructive Evaluation and Health Monitoring*. San Diego, CA, USA, Vol. 6928, pp. 692824.
- [9] Granstrom, J., Feenstra, J., Sodano, H. A., and Farinholt, K., (2007) "Energy harvesting from a backpack instrumented with piezoelectric shoulder straps," *Smart Materials and Structures*, **16**(5), pp. 1810-1820.
- [10] Yuse, K., Monnier, T., Petit, L., Lefeuvre, E., Richard, C., and Guyomar, D., (2008) "Self-powered Wireless Health Monitoring Supplied by Synchronized Switch Harvesting (SSH) Method," *Journal of Intelligent Material Systems and Structures*, **19**(3), pp. 387-394.
- [11] Anton, S. R., Erturk, A., and Inman, D. J., (2009) "Piezoelectric energy harvesting from multifunctional wing spars for UAVs: Part 2. experiments and storage applications," in *SPIE's 16th Annual International Symposium on Smart Structures and Materials & Nondestructive Evaluation and Health Monitoring*. San Diego, CA, USA, Vol. 7288, pp. 72880D-12.
- [12] Erturk, A., Anton, S. R., and Inman, D. J., (2009) "Piezoelectric energy harvesting from multifunctional wing spars for UAVs – Part 1: coupled modeling and preliminary analysis," in *SPIE's 16th Annual International Symposium on Smart Structures and Materials & Nondestructive Evaluation and Health Monitoring*. San Diego, CA, USA, Vol. 7288, pp. 72880C-15.
- [13] Dowling, N. E., (1999) *Mechanical Behavior of Materials: Engineering Methods for Deformation, Fracture, and Fatigue*, 2nd ed, Prentice Hall, Upper Saddle River, NJ.
- [14] Erturk, A. and Inman, D. J., (2009) "An experimentally validated bimorph cantilever model for piezoelectric energy harvesting from base excitations," *Smart Materials and Structures*, **18**(2), pp. 025009 (18 pp.).
- [15] Hagood, N. W., Chung, W. H., and Von Flotow, A., (1990) "Modelling of piezoelectric actuator dynamics for active structural control," *Journal of Intelligent Material Systems and Structures*, **1**(3), pp. 327-54.
- [16] du Toit, N. E. and Wardle, B. L., (2007) "Experimental verification of models for microfabricated piezoelectric vibration energy harvesters," *AIAA Journal*, **45**(5), pp. 1126-37.
- [17] Pereira, T., Scaffaro, R., Guo, Z., Nieh, S., Arias, J., and Hahn, H. T., (2008) "Performance of thin-film lithium energy cells under uniaxial pressure," *Advanced Engineering Materials*, **10**(4), pp. 393-399.
- [18] Pereira, T., Scaffaro, R., Nieh, S., Arias, J., Guo, Z., and Thomas Hahn, H., (2006) "The performance of thin-film Li-ion batteries under flexural deflection," *Journal of Micromechanics and Microengineering*, **16**(12), pp. 2714-2721.
- [19] Pereira, T., Zhanhu, G., Nieh, S., Arias, J., and Hahn, H. T., (2009) "Energy Storage Structural Composites: a Review," *Journal of Composite Materials*, **43**(5), pp. 549-560.
- [20] Erickson, W., and Maksimovic, D., (2001) *Fundamentals of Power Electronics*, Kluwer, Norwell, MA.
- [21] Kong, N., Ha, D. S., Erturk, A., and Inman, D. J., (2009) "Resistive Impedance Matching Circuit for Piezoelectric Energy Harvesting," *Journal of Intelligent Material Systems and Structures*, (submitted).